Forensic Analysis of Faulted NSTX-U Inner Poloidal Field Coil

Joseph R. Petrella, Jr., Irving J. Zatz, Stefan Gerhardt, Clayton E. Myers, and Mark D. Boyer

***Abstract*— The failure of the NSTX-U PF1A upper coil suspended plasma operations during the project's first operational campaign after commissioning. Initial nondestructive testing and examination of the failed coil was followed by extensive nondestructive radiography. Destructive testing facilitated visual borescope/videoscope inspection through the cooling path, vacuum testing, and electrical testing of every conductor segment. One conductor cooling path visually evidenced a void through the sidewall of the cooling path in a layer-to-layer region. The identified void in the conductor cooling path was not proximal to a braze or joggle. Electrical testing indicated that the voided conductor segment was a member of a group of 14 conductor segments that evidenced low-resistance connectivity. Four braze joints and two lead segments were subjected to 400-lbf/in^2 hydrostatic pressure testing followed by helium leak testing and evidenced that there were no detectable leaks in the tested cooling path segments. The faulted region was proximal to the center of the coil pack and evidenced historical electrical pitting and molten conductor debris. Samples of the epoxy resin insulation system were extracted and analyzed with dynamic mechanical analysis and differential scanning calorimetry techniques. Epoxy resin insulation samples were subjected to immersion testing per ASTM D570. Metallurgical samples were extracted from the coil pack conductors and subjected to hardness testing and grain structure analysis. The base material testing results indicated no abnormalities. The coil incipient failure was determined to most likely have resulted from conductive material located between conductor and insulation layers.**

***Index Terms*— Coils, magnetic confinement, maintenance, tokamaks.**

I. Introduction

ON JULY 22, 2016, the NSTX-U Project Team suspended plasma operations due to the inoperability of the PF1A upper (PF1A-U) coil. Preliminary indications evidenced that the PF1A-U coil experienced a coolant blockage. An external coolant leak developed from the PF1A-U coil pack after the blockage was attempted to be cleared.

Manuscript received June 28, 2017; accepted March 2, 2018. Date of publication June 6, 2018; date of current version July 9, 2018. This work was supported by the U.S. Department of Energy, Office of Science, Office of Fusion Energy Sciences, and has been authored by Princeton University with the U.S. Department of Energy under Contract DE-AC02-09CH11466. The publisher, by accepting the article for publication acknowledges, that the United States Government retains a non-exclusive, paid-up, irrevocable, worldwide license to publish or reproduce the published form of this manuscript, or allow others to do so, for United States Government purposes. The review of this paper was arranged by Senior Editor E. Surrey. *(Corresponding author: Joseph R. Petrella, Jr.)*

J. R. Petrella, Jr., I. J. Zatz, S. Gerhardt, and M. D. Boyer are with the Princeton Plasma Physics Laboratory, Princeton University, Princeton, NJ 08540 USA (e-mail: jpetrell@pppl.gov; izatz@pppl.gov; sgerhard@pppl.gov; mboyer@pppl.gov).

C. E. Myers was with the Princeton Plasma Physics Laboratory, Princeton University, Princeton, NJ 08540 USA. He is now with the Sandia National Laboratories, Department of Pulsed Power Sciences, Albuquerque, NM 87185 USA.

Color versions of one or more of the figures in this paper are available online at http://ieeexplore.ieee.org.

Digital Object Identifier 10.1109/TPS.2018.2831919

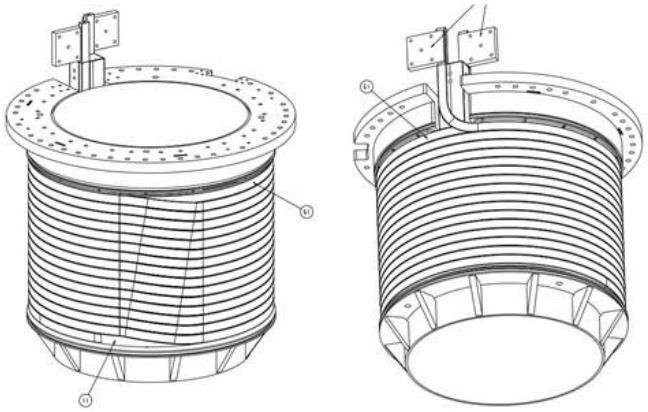

Fig. 1. Isometric representation of the PF1A-U coil.

II. Coil Characteristics

PF1A-U is a conventionally wound deionized water-cooled copper conductor electromagnet. The coil conductor is electrically insulated with layers of fiberglass and Kapton tape and wound on a stainless steel mandrel. The coil pack is vacuum pressure impregnated (VPI) with CTD-425 epoxy on the mandrel as an assembly. The coil conductor is approximately 440 ft long and has four in-line induction brazed joints. Turn density is maximized in the design by employing conductor joggles in turn transition regions. A representative schematic of the coil is shown in Fig. 1. The location of the PF1A-U coil on the center stack (CS) of NSTX-U is shown in Fig. 2.

III. Failure Characteristics

The PF1A-U coil was first put into service in August 2015 via the PPPL ISTP-001 process. Following the recommissioning issues unrelated to the subject investigation, the coil was put into service again in December 2015 via the PPPL ISTP-001 process. From January 2016 to June 27, 2016, PF1A-U operated without any detected incident for approximately 1000 shots of varying length and power. At no time, the coil was operated at the maximum design level. PF1A-U flexible bus deflections were observed on May 20, 2016. From May 23, 2016 to June 17, 2016, repairs were made to the PF1A-U flexible bus. Impact of the flexible bus deflections relative to the subject investigation was reviewed by the investigation team. After the review of the physical evidence and theoretical calculations, it was determined

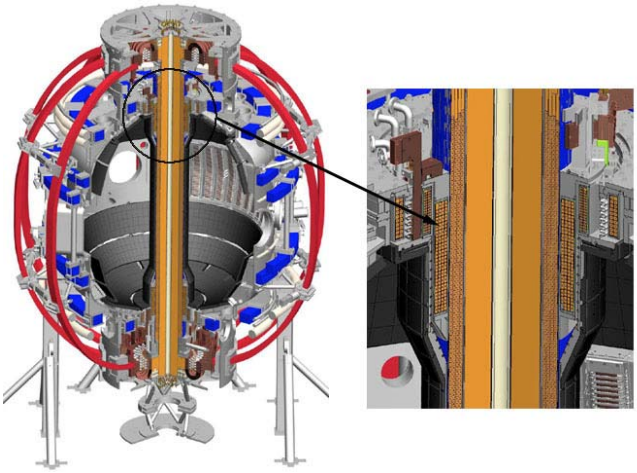

Fig. 2. Positioning of the PF1A-U coil on the NSTX-U CS.

that the flexible bus deflections did not impact the subject investigation. The flexible bus deflection incident is mentioned for completeness only.

On June 28, 2016, at approximately 16:05, the PF1A-U cooling path monitoring flow switch changed the electrical condition and evidenced a lack of cooling liquid flow. Diagnostic evaluation determined that this was not an issue with the flow sensor, but the coiling path within the body of coil was blocked/compromised. The coil electrical and water temperature waveforms were unremarkable leading up to the last shot attempted prior to the flow blockage detection.

Between June 30, 2016 and July 5, 2016, attempts were made to clear the blocked cooling path by various means including reversing flow. Coolant water recovered from PF1A-U was observed to be cloudy and evidenced particulate matter and a "charred" odor. A biological assay was performed on a sample of coolant liquid and evidenced levels of biological activity in initial samples. Coolant water from other coils was also sampled and tested and was unremarkable. The coolant path of PF1A-U was flushed with deionized water mixed with Dawn and subsequently Alconox. The blockage was reconfirmed to be within the body of the coil and not in the supply/return hoses. Each time the blockage appeared to have been cleared, the coil reclogged. Any resulting flow was far less than normal flow rates. On July 5, 2016, during 600-lbf/in^2 hydrostatic pressure testing of PF1A-U, water was observed coming from the bottom of NSTX-U. A copper/carbon slug was recovered from water which is used to flush the coil cooling path along with other debris. Chemical analysis of the slug showed that its component elements correspond with the composition of the conductor/epoxy/glass matrix but not the brazes (which would have shown evidence of silver and other elements). The conclusion at that time was that while a leak may exist at a braze, the slug was formed elsewhere.

On July 6, 2016, 15-lbf/in^2 pressure testing indicated that at least one blockage still existed in the coil with some of the results implying that there may be a second blockage. Drying of the NSTX-U vessel and coils proceeded following the leak event. Vacuum pumping on PF1A-U cooling paths yielded a frothy/bubbly liquid indicative of soapy water remaining within the cooling path of the coil. The decision was made to bake the entire CS, which includes PF1A-U. The bakeout process continued until July 19, 2016. During that time, periodic inspections evidenced frothy water within the PF1A-U cooling paths and water at the base of the CS.

IV. Flux-Loop Postmortem

From July 20, 2016 to July 22, 2016, limited operations resumed to include inductively energizing PF1A-U for the purpose of magnetically diagnosing the health of the coil. The primary magnetic diagnostics used in these tests were two poloidal magnetic flux loops, which were preinstalled loops of wire wrapped toroidally around the outside of the PF1A-U coil. These flux loops measured the toroidal loop voltage generated via Faraday's law when the poloidal magnetic flux passing through the loop changes in time. As such, when the loop voltage signal is integrated, the result is a time-resolved measurement of the poloidal magnetic flux passing through the loop.

Since the two flux loops were attached directly to the PF1A-U coil, they were highly sensitive to toroidal currents flowing in the coil. Thus, during July 20, 2016–July 22, 2016 recommissioning period, the objective was to apply an inductive loop voltage to the PF1A-U coil by ramping a nearby magnetic field coil (PF2-U). If the PF1A-U coil was compromised, the applied loop voltage would induce anomalous currents in PF1A-U that would be detected by the magnetic flux loops. During these tests, transient induced currents within PF1A-U were observed. This was the first direct indication that the coil was electrically shorted internally. These results motivated a more thorough investigation of induced PF1A-U currents during the preceding months of operations.

The induced PF1A-U coil currents generated during routine plasma operations can be retrospectively assessed because the ohmic coil (the central solenoid) applies a consistent loop voltage to the PF1A-U coil immediately before each plasma discharge. More specifically, the ohmic coil is ramped to a precharge current of $+20$ kA before the initiation of the plasma. This ohmic current ramp applies the same $\sim$2 V of inductive loop voltage to the PF1A-U coil in every discharge. As such, the PF1A-U flux-loop measurements could be examined over several months of operations to determine if currents were being induced in an electrical fault in the PF1A-U coil. Fig. 3 illustrates the total induced current in PF1A-U as inferred from the poloidal flux-loop measurements. These data are obtained by computing the mutual inductance coupling matrix between the two flux loops and the coil and then inverting the coupling matrix to extract the coil current. The PF1A-U induced current measurements [Fig. 3 (blue)] show a clear degradation that begins toward the end of the March/April run period. This degradation continues through the May and June run periods and then accelerates rapidly on the final run day before operations were halted. Approximately 100-kA turns of current were induced in PF1A-U during the ohmic precharge for the final plasma shot. Similar measurements for the PF1A lower (PF1A-L) coil [Fig. 3 (red)]

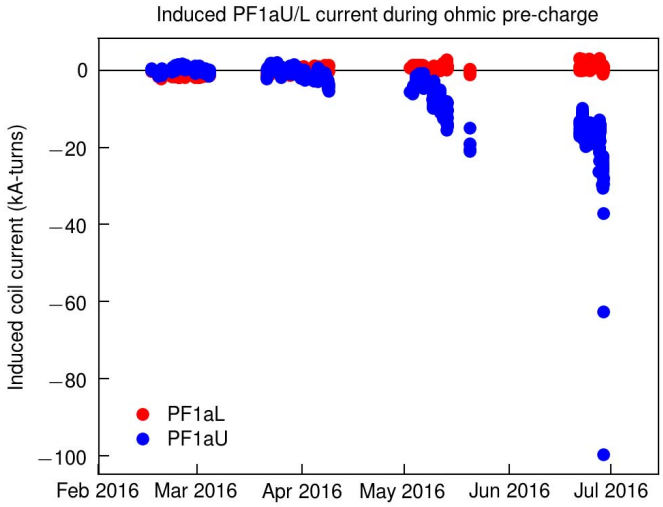

Fig. 3. Gradual change in the inductance of PF1A-U over time.

show that PF1A-L did not experience any degradation over the course of the run. On July 22, 2016, PF1A-U operations were suspended.

V. Nondestructive Testing

The PF1A-U coil was removed from the NSTX-U CS on August 24, 2016. It was safely lifted, without incident, out of the test cell and onto a platform in the South High Bay. The coil was surveyed for radiation activity and cleared by health physics.

A. Visual Inspection

The PF1A-U was visually examined and extensively photographed in the South High Bay. It was noted that portions of the observable surfaces evidenced a powdered deposit indicative of dried sediment. An external visual inspection of the coil conductor leads was unremarkable. A majority of the electromagnet was not visible due to the shields that cover the perimeter of the coil. These shields are welded to the upper and lower flanges of the mandrel. Nevertheless, areas of surface delamination and discoloration were observable in the gaps between the shields.

B. Initial Electrical Tests

Prior to the removal of the shields, the lead-to-lead electrical coil resistance was measured with a Megger 10-A digital low resistance ohmmeter micro-ohmmeter to be 5.942 mΩ on August 24, 2016. High-pot electrical tests at voltages ranging from 500 to 5000 V were performed, and the data were recorded for comparative purposes (Table I). The shields were then removed with a die grinder, thereby exposing the overall circumferential surface of the coil pack (Fig. 4). High-pot electrical tests at voltages ranging from 500 to 5000 V were repeated on the shieldless coil on August 26, 2016, and compared to the previous tests. The comparison of the electrical tests was unremarkable. It is noteworthy that on June 6, 2016, approximately one month prior to the blockage event, the leakage current was measured to be 9 μA at 5 kV.

TABLE I
PF1A-U Postremoval Electrical Tests

Tests performed on 08/24/2016 & 08/26/2016								
No water connected to coil								
Coil Resistance		5.942 milliohms		(10A DLRO)				
The coil case was grounded and coil leads shorted. Then the coil was hipotted to the case.								
		8/24/2016				8/26/2016		
Volts		**Leakage uA**				**Leakage uA**		
500		40				21		
1000		60				39		
1500		90				60		
2000		110				75		
2500		125				95		
3000		140				100		
3500		155				100		
4000		170				105		
4500		180				120		
5000		230				140		
	decayed to	170	after one minute			120	after one minute	

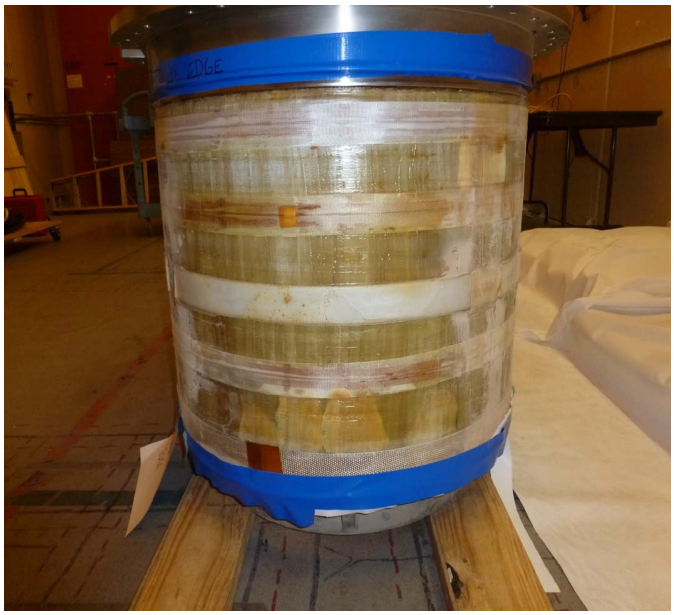

Fig. 4. PF1A-U exterior with shields removed.

C. Visual Inspection Postshield Removal

Fig. 5 illustrates a focused view of the outside surface of the PF1A-U coil. Short, dark vertical lines were observed that evidence separations/tears in the ground layer wrap. An internal coolant path leak in the electromagnet may communicate with these separations as potential exit points for coolant. Removal of the shields evidenced numerous ground wrap delamination areas identified by their lighter color and confirmed by lightly tapping the areas with a tool that audibly noted hollows beneath the ground layer.

D. Radiography and Low-Pressure Test

On August 30, 2016, the PF1A-U coil/mandrel was transported by PPPL truck to Mistras Group, Inc. (Mistras), Marcus Hook, PA, USA, and staged for gamma radiographic examination. On September 1, 2016, Petrella traveled to Mistras to observe a radiographic study of the PF1A-U. Mistras personnel employed an iridium-192 radioisotope source to irradiate

Fig. 5. PF1A-U ground wrap delamination.

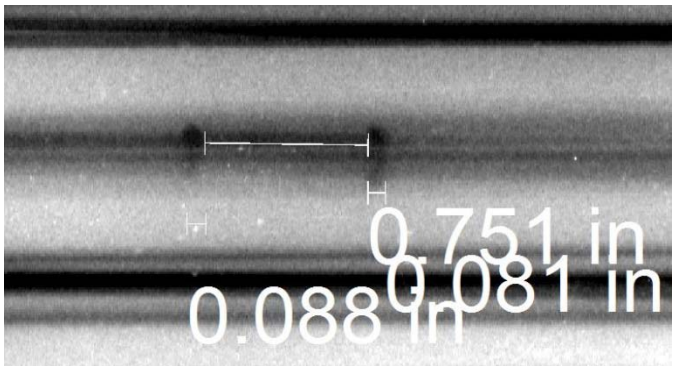

Fig. 6. Radiographic image of braze joint 4.

14×17 in^2 photostimulable phosphor plates placed in angular segments around the exterior of the PF1A-U coil. The exposed phosphor plates were digitized in a virtual media integration (VMI) model 5100MS-C plate scanner. The PF1A-U exterior circumference was marked with eight angular regions labeled "0"–"7," and a symmetric centerline was designated proximal to the midplane of the coil pack. Image segments located above the midplane area toward the lead-out flange were designated "A," and images below the midplane proximal to the tapered end of the mandrel were designated "B." Correspondingly, recorded images were identified in segmental fashion, i.e., "image 0_1A." A total of 19 images were recorded during the September 1, 2016 imaging session with scale reference. Images were surveyed for anomalies by Mistras representatives using VMI Starrview 8.0 NDT software. The September 1, 2016 survey identified four anomalies with signatures indicative of in-line braze joints (Fig. 6). The locations of these anomalies corresponded proximally to the locations identified in the manufacturing process outline (MPO)/traveler provided by the coil manufacturer, Everson Tesla, Inc. In addition, the September 1, 2016 survey identified an anomalous region proximal to the midplane of the coil pack section at the angular proximity of the lead-in/lead-out area.

On September 8, 2016, Petrella again traveled to Mistras to observe a resurvey of the anomalous region and employ a

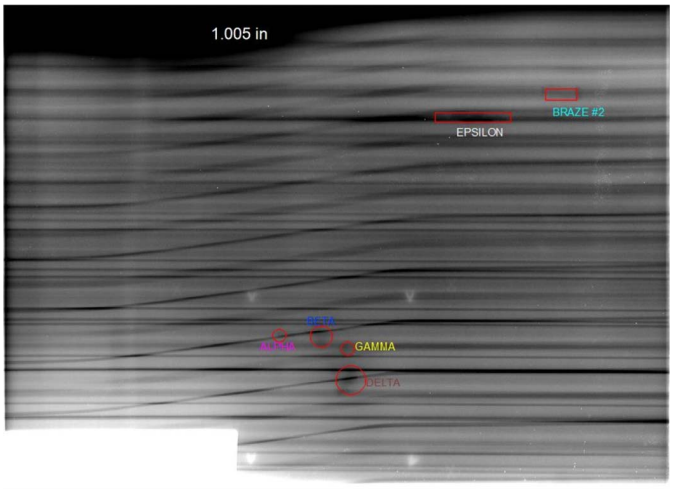

Fig. 7. Approximate references for anomalies identified in region 0_1A.

triangulation analysis method developed at PPPL for determination of the radial position of the anomalies. Scale paper templates were used to position reference indices and the iridium-192 radioisotope source to create an intentional 25° parallax of the anomalous region. A total of 13 new images were recorded and were indexed in a similar fashion to the previous radiograph images with scale reference and the addition of a parallax notation. The scaled images were digitally imported into an AutoCAD drawing. The anomalous regions angularly proximal to the lead-in/lead-out area were divided into visually perceivable density variations "alpha" through "epsilon" (Fig. 7). In-line braze joint 2 was visible in the imaging and was also included in the triangulation analysis. Circles and rectangles were drawn over the observed density variations to optically determine an approximate center point reference for each area. A triangulation analysis was performed to determine proximate radial positions of the observed anomalies. The analysis indicated that the regions alpha through gamma were proximal to conductor rows 8 and 9 and between conductor layers 2 and 3. The analysis also indicated that braze joint 2 was radially proximal to layer 2. This geometric approximation corresponded to the Everson Tesla, Inc. (ETI) MPO documentation for braze joint 2, validating the radial positional interpolation of regions alpha through epsilon.

Further validation of the triangulation method was performed by surveying in-line braze joint 1 with the triangulation approach and comparing the results with the ETI MPO. The geometric approximation using the triangulation imaging technique proximally identified braze joint 1 in the reported radial position, thereby further validating the triangulation method used.

The completed radiographic study was used to select locations to segment the coil for destructive evaluation. The features observed in the radiographic study allowed the investigation team to minimize the risk of compromising anomalies and critical areas such as brazes, joggles, and leads.

Low-pressure testing of the entire intact coil was the final nondestructive step prior to segmenting the coil pack. Nitrogen gas was used to charge the PF1A-U cooling path to approximately 15 lbf/in^2 to determine if the cooling paths evidenced

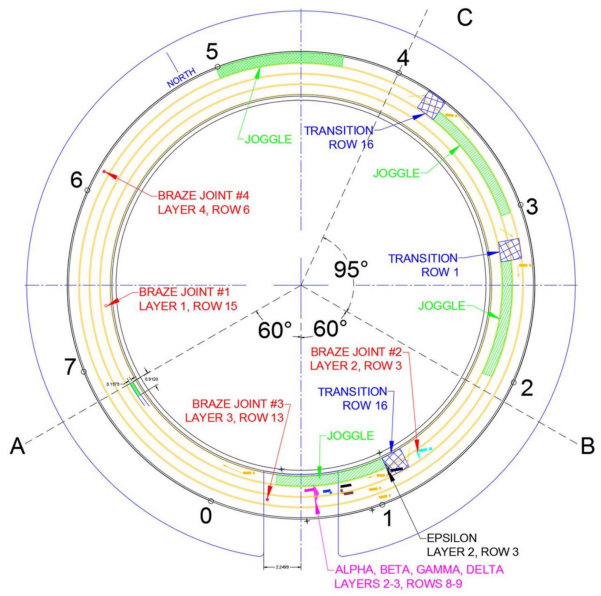

Fig. 8. Identified sectioning cuts "A, B, and C."

low-pressure leaks postremoval from NSTX-U. Four scenarios were tested and indicated that the coil cooling path did not have a gross leak to atmosphere, but debris existed in the leak path causing the flow through the cooling path to be intermittent.

VI. Destructive Testing

A. Coil Sectioning

A peer review was held on September 19, 2016, to establish consensus on the proposed destructive testing plan based on the results of the radiography. Determination of the origin and extent of the internal anomalies observed in the radiographic survey necessitated visual and physical access to individual PF1A-U conductor segments. The combined, observed, and deduced locations of braze joints and anomalies guided the selection of three feature-free areas for segmentation of the coil pack. The three sectioning cuts were proposed and identified as cuts "A," "B," and "C" as noted in Fig. 8. Section A_B would be of the greatest interest because it contained the five principal anomalies, alpha through epsilon, identified by radiography, plus the leads and two of the four braze joints.

The method of segmenting the coil pack was examined in parallel to the locations of segmentation and presented at the peer review. A decision matrix was developed to guide the segmentation method selection process. The highest (best) scoring option was determined through the decision matrix to be a milling process using a rotary end mill without lubrication. The proposed segmentation process and destructive testing plan was agreed to by consensus at the peer review. Once segmented, the coil sections would be subjected to borescope inspections, electrical tests, vacuum tests, and pressure tests. A procedure was written and approved to employ the milling segmentation technique and outline the steps to demandrel the milled coil pack sections. In addition to the procedure, a drawing set was generated to specify the cut locations, parameters, and fixtures. All efforts were made to select coil pack cutting planes that avoided identified anomalies, braze joints, and joggle areas. Layer transitions were not able to be identified in the radiographic study due to the transition being out of plane with the imaging.

Coil pack retention fixtures were mounted on the PF1A-U and the assembly crane-lifted onto a horizontal Lucas Mill table. Two dedicated, new, marked shop vacuums were used to collect milled debris from each cutting plane during the machining process. These shop vacuums were used to retrieve debris from their designated cutting plane throughout the segmentation process, with the exception of specific collections of noted debris. A 5/8 in cobalt four-flute end mill was used to mill the cutting planes. The milling process removed approximately 31.9 in^3 of coil pack volume at each of the three cutting planes for a total of 95.83 in^3 of removed material. The approximate total volume of the PF1A-U coil pack is 4102.48 in^3. The amount of material removed during the milling process was therefore approximately 2.34% of the coil pack volume. Despite the small proportional amount of material removed from feature-free regions, each cutting plane was cautiously milled in 0.03-in increments and inspected for anomalies after each milling pass. The machinist stopped milling as well as notified the Accountable Technical Individual if any anomalies were observed.

B. Coil Pack Section Removal

The segmented PF1A-U assembly was crane-lifted from the horizontal Lucas Mill and placed on a Ransome rotary/tilt table. Fixtures were loosened/displaced to enable the radial displacement of coil pack sections B_C and C_A. Spacers and wedges fabricated from G-10 were inserted into the cutting planes to progressively force the coil pack section(s) away from the mandrel. The removed coil pack sections were placed and cribbed on tables for examination and testing. After photographing the general conditions of the six exposed cutting plane surfaces, a conductor number was assigned to each conductor segment at one side of the coil pack segment. The conductor number designated the "starting" location at one cutting plane, whereas the connected, opposite conductor number would be the same conductor segment but not necessarily in the same vertical or radial relative location due to the winding pattern. The opposing matching conductor location was determined during subsequent electrical and vacuum tests and marked accordingly. Coil pack section A_B was not removed from the mandrel in order to limit any potential disturbance to the radiographed anomalies previously identified as alpha through epsilon located proximal to the lead-in/lead-out angular position.

Exterior visual examination of cutting planes A and C, left and right, evidenced insulation anomalies that were also observed during the milling process (Fig. 9). Cutting plane B, left and right, evidenced a separation between conductor layers 2 and 3 from approximately conductor row 3 to conductor row 16. Observed conductor spacing, insulation characteristics, and conductor keystoning were noted and

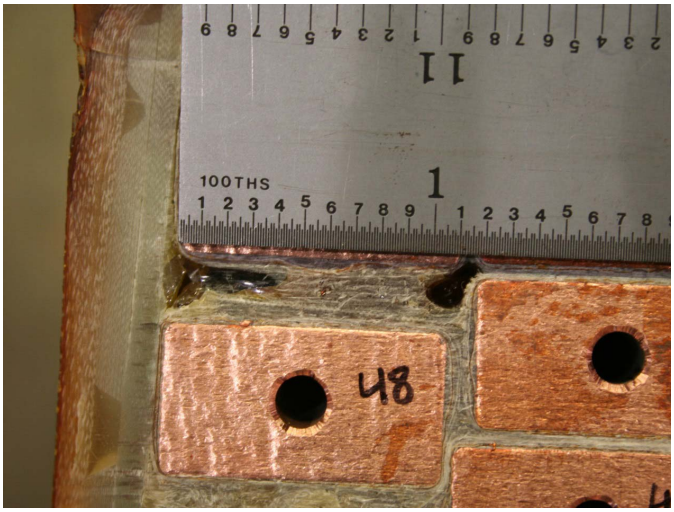

Fig. 9. Coil pack section plane C void.

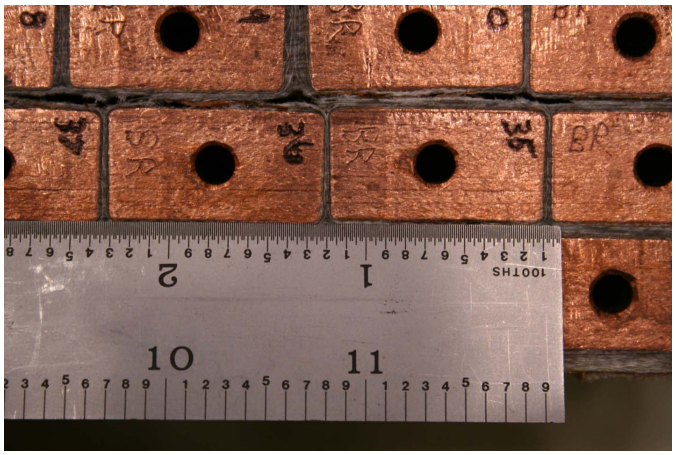

Fig. 10. Coil pack section plane B keystoning.

photographed (Fig. 10). Examination of the insulation wrap sequence evidenced that each conductor was wrapped with a half-lap co-wound glass/Kapton layer with the glass portion laid up against the conductor surface. A glass-only half-lap layer was observed to be wound over the co-wound glass/Kapton layer. Each layer-to-layer region evidenced an additional flat-laid glass layer.

C. Borescopic/Videoscopic Inspection of Coil Sections

Interior visual examination of each coil segment cooling path was performed with both fiber borescope and digital videoscope. The borescope used is a PPPL owned basic eyepiece device without recording capability with a limited viewing range. An Olympus IPLEX IV9435 RX videoscope was rented for a one-week period. This Olympus videoscope had a focus range of 2 mm with both forward and side view attachments. In addition, the videoscope could be viewed on a screen with both still and video digital recording capabilities.

Each coil segment cooling path was surveyed for visual anomalies and photographed and videoed with the Olympus videoscope if anomalies were observed. It is noteworthy that

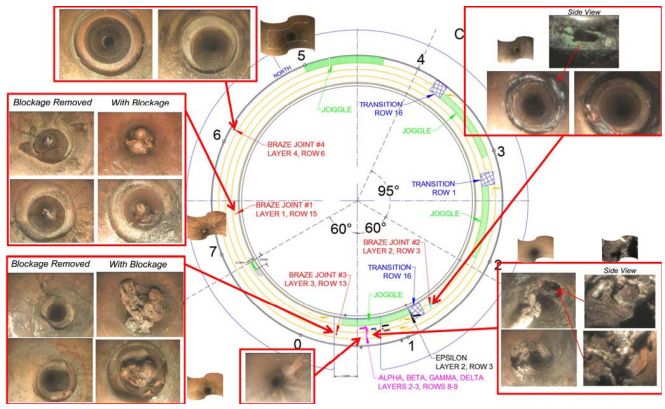

Fig. 11. Borescope findings compilation.

the braze joints and anomaly "delta" (features visible from the cooling paths) radial positions predicted in the radiographic triangulation method were accurate and verified through the cooling path visual examination. A compilation of findings mapped to a plan view of the PF1A-U coil is illustrated in Fig. 11.

D. Electrical Testing

A grounding harness consisting of copper wire and banana plugs was inserted into the cooling path of each conductor along one side of each coil pack section for megger testing. The conductor under test was electrically disconnected from the grounding harness during the test. Each conductor segment was megger tested at 250 VDC. The observed conductor insulation resistance varied from 1.81 MΩ to greater than 750 GΩ in unshorted conductor segments.

A total of 14 conductor segments were observed to be effectively shorted in coil pack section A_B. Additional turn-to-turn resistance measurements were performed between these electrically communicating turns and varied from 0.5 to 17.4 Ω.

E. Vacuum Testing

A low-vacuum pump was configured with a moisture/debris trap in order to selectively apply vacuum to conductor segment cooling paths. Each cooling path segment was vacuum tested at approximately 29 in of mercury for 2 min. One conductor segment cooling path failed to hold vacuum. The leaking conductor section was determined to be the cooling path with the internally observed void (section A_B, layer 3, row 9, and conductor No. 41).

F. Pressure Testing

The cooling paths of conductor segments containing braze joints and leads were tapped with a 1/8-in NPT tapered thread for the attachment of pressure testing components. A 15-lbf/in^2 nitrogen pressure test was followed by a 400-lbf/in^2 hydrostatic pressure tests for each tested conductor segment. Hydrostatic tests were repeated to vet out setup variances, including subjecting one test setup to an overnight leak down. All four tested braze joints and leads passed

Fig. 12. Layer 3 surface with debris overview.

Fig. 13. Layer 2 surface with debris overview.

hydrostatic testing at 400 lbf/in^2. Low-pressure helium leak tests were additionally performed on the conductor segments featuring the leads, braze joint 2 and braze joint 3 in section A_B, and were unremarkable.

G. Exposure of Faulted Area

Coil pack section A_B, which contained the fault area, remained on the mandrel for the duration of the previously described tests to ensure minimal compromise of the fault area. Removal of the coil pack was performed in a similar fashion as the previously removed coil pack sections, B_C and A_C, and was uneventful. The authors noted that the sprue hole locations were readily discernible along the coil pack ground wrap by sheared "neat" white resin deposits.

A means to split the coil pack along the layer-to-layer region between layers 2 and 3 was devised employing a custom fabricated splitting fixture. The conductor cooling paths along layers 2 and 3 were tapped to permit the attachment of the splitting fixture. A relief cut was made in the ground wrap to provide a preferential parting plane between layers 2 and 3. The leads were removed to aid in splitting the coil pack section.

The splitting fixture, a hydraulic ram, dial indicator, and resistance monitor (between layers 2 and 3) were attached to the coil pack section to facilitate splitting layers 2 and 3. Electrical isolation of the two coil pack halves was maintained during the splitting process to allow the monitoring of resistance between layers 2 and 3 during the splitting process. The layer-to-layer resistance did not appreciably change during the splitting process and simply increased to infinity when the layers became fully separated. The turn-to-turn resistances of layers 2 and 3 conductors adjacent to each other did not appreciably change after the layers were split.

The coil pack section A_B was split between layers 2 and 3 to expose the electrically affected area.

An area of damaged electrical insulation was observed that measured approximately 10 in in height and 12 in in length (toroidally) between layers 2 and 3 (Figs. 12 and 13). Areas of unwetted woven glass fibers were observed proximal to the damaged region (Fig. 14).

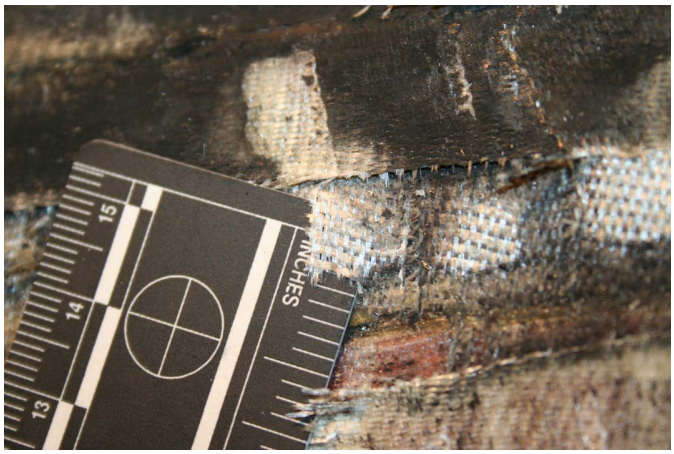

Fig. 14. Unwetted woven glass fibers.

A primary electrical activity area was observed proximal to conductor turns No. 40 and 41, with a void located in the sidewall of conductor No. 41 along the cooling path in layer 3 facing layer 2 (Fig. 15). This void was previously documented as viewed from within the conductor cooling path. The opposing layer 2 area evidenced pitting but no breakthrough to the cooling channels (Fig. 16). The observed pitting was characteristic of electrical activity occurring along the outer surfaces of the conductor(s). The void in the sidewall of conductor No. 41 would therefore have evolved from the conductor surface and extended into the cooling path over time. Solidified molten debris was observed surrounding the void in conductor turn No. 41 and appeared to exhibit an impression of the woven glass fiber insulation. Spherical globules of molten debris, some adhering to the conductor surfaces, some loose, were also observed. Loose debris was removed from the void area, evidencing adhered molten globules as well as areas of oxidation along the exposed conductor surfaces. Cavities were observed in conductor turn No. 40 adjacent to the void in conductor No. 41. Macroscopic examination of the void in conductor turn No. 41 evidenced varying extensive pitting and localized varying oxidation, indicative of repetitive historical electrical activity (Fig. 17).

A secondary electrical activity area was located along conductor turns No. 30 and 36 (Fig. 18). The electrical

Fig. 15. Layer 3 void area with debris overview.

Fig. 16. Layer 2 area opposite layer 3 void with debris.

activity in this area was not oxidized nor did it evidence significant pitting, indicating that this area of activity occurred near or after the time of the ultimate failure. The authors noted that the subject coil was inductively energized after the ultimate failure for diagnostic purposes, and the authors cannot rule out the possibility that the secondary electrical activity may have occurred during these tests. The secondary electrical activity area was likely initiated by migrating debris and liberated cooling fluid after the ultimate failure of conductor No. 41.

It was observed that the resin injection and overflow sprue holes were not aligned with machined insulation shims installed along the upper and lower ground-plane interface with the mandrel impeding the resin injection path. It was

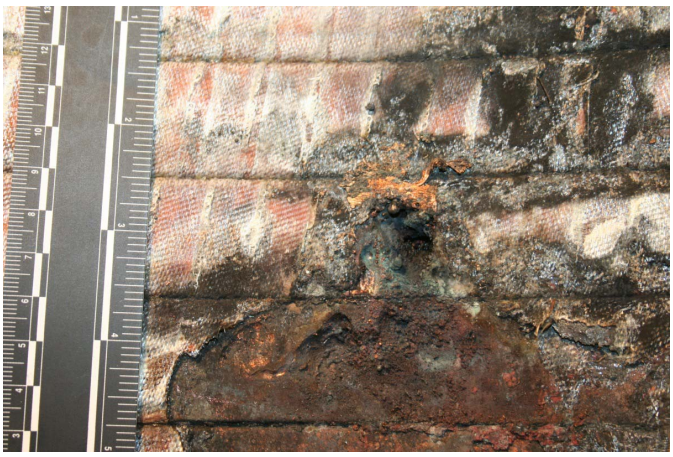

Fig. 17. Layer 3 void with loose debris removed overview.

Fig. 18. Layer 2 conductor No. 30 electrical activity.

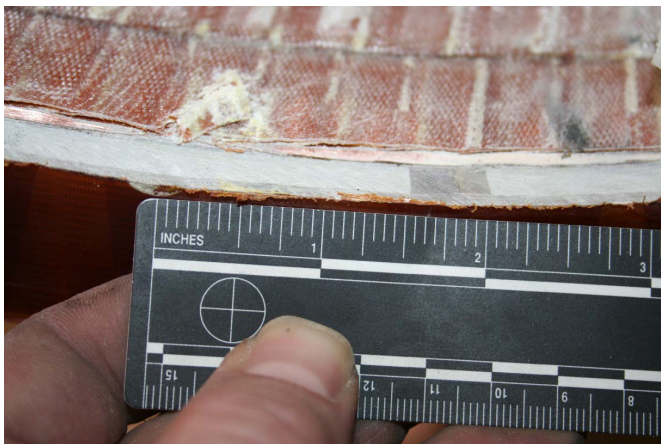

Fig. 19. Resin vent sprue mandrel versus G-10 offset.

observed that the lead-side insulation shim/mandrel sprue openings were offset approximately 1–3/4 in (Fig. 19). The lead-opposite insulation shim/mandrel sprue openings evidenced an offset of approximately 5/8 in. The insulation shim

Fig. 20. Resin globules along layer 3 bottom turn.

fabrication drawing indicates that the same shim design was used for both PF1A-U and PF1A-L. However, the PF1A-U and PF1A-L stainless steel mandrels, and their corresponding sprue hole locations, were not identical. A 7.5° toroidal angular difference in sprue hole location was identified according to the mandrel fabrication drawings. This angular difference accounts for an approximate 1.66-in misalignment in the lead-side PF1A-U insulation shim sprue holes verses the stainless steel mandrel sprue holes. However, the design documentation does not account for the lead-opposite sprue hole alignment.

VII. Material Testing

Samples for metallurgical and chemical analysis were extracted from coil pack section B_C. The ground wrap insulation system was able to be separated from the three portions of the coil pack by inserting a wedge in between the conductor insulation wrap and the ground wrap. The resin fill density was observed to be inconsistent, forming into globules in resin-rich areas (Fig. 20).

Insulation samples were removed from well-wetted regions of the inner ground wrap insulation and labeled 1, 2, 3, A, and B. Insulation samples were also removed from well-wetted regions of the outer ground wrap insulation and labeled 4, 5, 6, C, and D. Note that Sample D intentionally included a portion of Hysol-adhered reinforcing wrap. A resin-rich "neat" resin sample was removed from a region close to a fill sprue location. Samples 1–6 were used for ASTM D570 immersion testing to determine the absorption characteristics of the composite. The percent increase in weight was found to be typical of similar glass-resin composites with an average increase in weight of 0.24%.

Samples A–D were used for dynamic mechanical analysis (DMA), and the "neat" sample was used for differential scanning calorimetry (DSC). The insulation system DMA and resin DSC characteristics were found to be typical for the material examined. It was observed that Sample D evidenced two tan delta peaks indicative of a sample containing more than one resin system. This was an anticipated result as Sample D included a Hysol-adhered reinforcing wrap.

In order to reconcile questions that have been raised regarding the integrity of the conductor material used to fabricate the PF1A coils, metallurgical samples were prepared for examination by an independent qualified testing laboratory. Metallurgical samples were removed from coil PF1A-U pack section B_C conductor turns No. 40–42, all proximal to the location of the sidewall failure in turn No. 41. Samples were taken from both the straight sections and joggles of these turns. In addition, control samples were taken from excess material remaining from the original lot of copper conductor.

A total of eight samples were tested (three straight, three joggles, and two control). The samples were delivered to Laboratory Testing, Inc., Hatfield, PA, USA, an accredited Nadcap (National Aerospace and Defense Contractors Accreditation Program) facility. The samples were subjected to micrograin and microstructure examinations at various magnification resolutions for grain size, microcracking, and evidence of cuprous oxide. In addition, Rockwell hardness measurements were taken of the samples.

Grain sizes and hardness were found to be typical for the base copper material. No evidence of cuprous oxide was observed. No evidence of microcracking was observed. No grain recrystallization was found. These findings apply to all samples tested. The conclusion from these tests is conclusive that the conductor material was not metallurgically compromised in any way in both its original as-delivered state from the mill and postfabrication state in the PF1A coils. The metallurgy of the copper conductor, therefore, is not considered a contributing cause to the failure of the PF1A-U coil.

VIII. Conclusion

Based on the investigation observations and by a process of elimination, the following conclusions can be reached.

1) The failure of the subject coil was progressive over time and involved conductors between layers 2 and 3.
2) The ultimate failure was located within the sidewall of conductor No. 41 along layers 2 and 3. It is probable that the initiating failure originated in the proximal area of the ultimate failure was electrical in nature and propagated from the surface of the conductor into the cooling path.
3) It is probable that electrical activity at the void location resulted in molten debris that blocked the cooling path at restrictions in the conductor braze joints.
4) Communication of debris into the conductor electrical insulation system most likely resulted in the observed low-resistance connectivity to 13 other conductor segments.
5) Metallurgical and materials testing performed on samples removed from the coil pack indicate that it is unlikely that a base material defect in the conductor or resin contributed to the initiating failure.
6) Misalignment of the insulating shim and mandrel sprues likely impeded resin flow during the VPI process. The lead-side sprue misalignment is attributed to a design variance while the lead-opposite sprue misalignment is likely to have occurred during assembly.

7) The probable cause of the initiating failure was the electrical bridging of conductors via the presence or formation of conductive material that penetrated the layer-to-layer insulation system. The conductive material may have been comprised of a solid or liquid substance. Heat as a by-product of the resulting electrical activity between layer conductors eroded the conductors over time. Eventually, a void was eroded in conductor No. 41 through to the cooling path, resulting in the migration of debris within the cooling path as well as between layers 2 and 3 of the coil pack. Empirical verification of this probable cause is highly improbable as the evidentiary region was consumed and compromised in the ultimate failure as well as being flushed postfailure with various solutions *in situ*.
8) The initiating failure was not directly caused by the observed under-performing VPI. However, it is probable that the under-wetted insulation system was a contributing factor to the initiating failure. The observed condition may have given opportunity for the presence and/or migration of conductive materials through the insulation system as well as allowing mechanical abrasion of the insulation system to occur.

Authors' photographs and biographies not available at the time of publication.